ADVANCED MATERIALS TECHNOLOGIES

www.advmattechnol.de

Ultrastrong and High-Stroke Wireless Soft Actuators through Liquid–Gas Phase Change

Mustafa Boyvat, Daniel M. Vogt,* and Robert J. Wood**

Soft actuators and robots, which depart from classical paradigms in rigid robot construction, increase the safety of robot–human and robot–environment interactions, bring superior adaptation capabilities, and extend the range of robotic operations to fragile and sensitive objects and environments. Pneumatic soft actuators are a key building block for soft robotics due to their inherent simplicity, high forces, and large strokes. However, pressure lines connected to large pumps, regulators, and valves put significant mobility limitations on these actuators. Recently, it has been demonstrated that by using phase changes of liquids, pumps can be eliminated in favor of on-board pressure generation. Here, it is shown that power and control of soft actuators can be realized through phase change of liquids stimulated by inductor-capacitor resonant receivers placed in an external magnetic field. The method requires no pumps, no external fluidic or electrical wiring, and no batteries on-board, leading to the possibility of small and low profile wireless soft actuators and robots which can operate for long durations. The phase change enables ultrahigh forces and high strokes with a small volume of active material. An ultralow profile, strong and soft pneumatic bellows-style actuator powered and controlled wirelessly demonstrates the potential of this technique.

1. Introduction

Rigid mechanical components used in traditional robots limit their use in tasks involving interaction with sensitive objects. Soft actuators and robots have been able to handle sensitive objects safely and offer high adaptation capabilities, making them promising candidates to overcome the limitations caused by rigid materials.[1–7] While there are several actuator options to use, their potential to have large forces, high strains, and fabrication simplicity have made pneumatic soft actuators ubiquitous in soft robotics.[6–8] However, actuation is typically accomplished by pressure lines, large pumps, regulators, and valves that impose significant limitations on their mobility.[6] Recently, there has been considerable interest in this issue and it has been demonstrated that use of phase change in liquids for on-board pressure generation can be a simple and effective replacement for pumps.[9–19] The method is based on vapor production inside the actuator through heating by electrical power to obtain the necessary pressure.[10–12,16,19] However, in those examples power and control have been achieved either by external electrical connections to an off-board power source or using an on-board battery. Batteries and external wire connections hinder the use of robotic devices significantly and thus wireless power and control of robotic agents has been a topic of interest recently.[20–23]

Following the demonstration of folding-based small wireless robotic devices equipped with shape memory alloy actuators, small pneumatic wireless soft actuators actuated by the pressure produced by liquid–gas phase change are expected to provide another useful component for compact battery-free wireless actuation.[23]

In this work, we demonstrate that the advantages of pneumatic soft actuators can be conveyed to battery-free wireless robots. By removing the necessity of external power connections and batteries through the use of magnetic fields to control a phase change in the internal working fluid—a method that differs from previous studies using phase change materials—we demonstrate the feasibility of ultralow profile, light, wireless soft actuators exhibiting large stroke and high output forces.[10–12,16,19] The fabricated prototypes, including the on-board electronics and the working liquid, weigh 1–2 g and are as thin as 2–3 mm before actuation. These prototypes can apply forces up to ≈1000 times their weight and can extend to approximately eight times the initial thickness (see **Figure 1** and Movie S1, Supporting Information).

2. Results

2.1. Concept

The method is based on changing the pressure in an actuator by evaporation and condensation, i.e., a phase change. A liquid is placed inside the actuator and an electrical heater is put in contact with the liquid to evaporate it (see **Figure 2**a). The power is transferred wirelessly to an inductor-capacitor (LC) resonator formed by a conductive coil connected to a capacitor. When sufficient power is supplied, the heat produced in the resonator triggers an accelerated evaporation with associated expansion. A load can also be connected to the resonator for additional power and heating adjustment. The increased pressure

Dr. M. Boyvat, D. M. Vogt, Prof. R. J. Wood
60 Oxford Street, Cambridge, MA 02138, USA
E-mail: mboyvat@fas.harvard.edu; dvogt@seas.harvard.edu; rjwood@seas.harvard.edu

The ORCID identification number(s) for the author(s) of this article can be found under https://doi.org/10.1002/admt.201800381.

DOI: 10.1002/admt.201800381

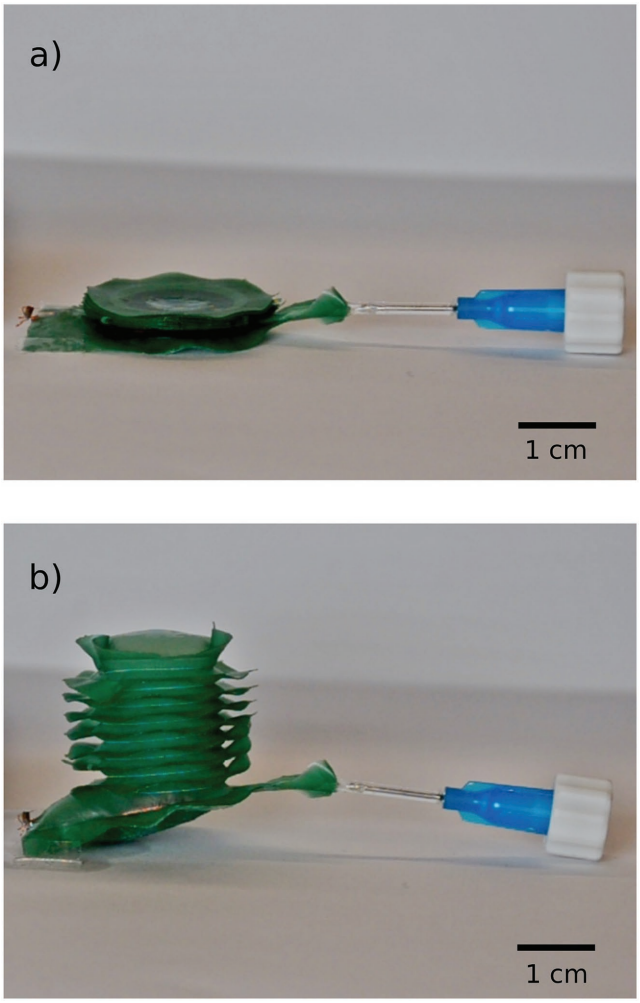

Figure 1. A wireless ultrathin bellows-style actuator before and during actuation. The thicker connection is kept to ease filling by a syringe and is not an essential part of the actuator. a) Before actuation. b) During actuation.

inside the actuator yields expansion and/or force (see Figure 2b). The contraction of the actuator happens by cooling. When the power is switched off and the vapor loses heat, the pressure inside the actuator drops as the gas condenses.

The working principle of the wireless power transmission is based on Faraday's Law. An external time-varying magnetic field induces a voltage in the coil and this can be written in the phasor domain as

$$V = -\sum_{n=1}^{N} j\omega\phi \tag{1}$$

where V is the induced voltage, $\omega = 2\pi f$, f is the frequency of the field, and ϕ is the magnetic flux through each loop forming the coil, which is $\iint_A \mathbf{B} \cdot \boldsymbol{dA}$. Here, $\boldsymbol{B}$ is the magnetic flux density vector and $\boldsymbol{dA}$ is the differential area vector. The current in the resonator can be calculated in phasor domain by $I = V/Z$, where I is current and Z is impedance. The impedance of a series LC circuit is given by $Z = j\omega L + 1/(j\omega C) + R$, where L is the inductance, C capacitance, and R total resistance. When the frequency of the external field is equal to the resonant frequency of the resonator, the impedance takes its minimum value in a series LC circuit and current reaches maximum, assuming a constant induced voltage and R, L, and C values. This also results in the maximum heat transfer to the load (the surrounding liquid) at resonance for a given induced voltage and constant component values. The dissipated power P_r at the resonant frequency in the resonator can be calculated by $P_r = I^2 R$. The heat produced by the resonator causes the liquid inside the actuator to evaporate and increase the pressure in the actuator, leading to force and/or motion depending on the external mechanical load. After power is switched off, the condensation process starts. The ambient temperature, environmental conditions such as air flow, the thermal conduction of actuator walls, and the temperature of the heater when the power is switched off can play role in determining cooling time.

2.2. Bellows Fabrication

The bellow actuators are made by stacking up sheets (**Figure 3**a,b) of TPU (thermoplastic polyurethane) and using masks made of polytetrafluoroethylene (PTFE/Teflon), to define where the TPU layers are bonded.[24] Both TPU layers and Teflon masks are cut using a CO_2 laser, and all the layers are aligned using dowel pins with precision die plates as shown in Figure 3c. Once stacked, TPU layers and Teflon masks are kept in an oven at 170° for 1 h and 30 min under a 1 kg weight.

The lower layer of the actuator (Figure 3d) is designed such that a large opening is available for inserting the resonator. A liquid inlet is also present to allow for filling of the actuator with the low evaporation point liquid. Both of these openings can then be sealed with an impulse heat sealer (AIE-410FL, American International Electric Inc., City of Industry, California, USA) to ensure that the actuator is airtight.

2.3. Characterization

Figure 4a shows an experimental characterization of the output force versus pressure difference for a bellows actuator with no resonator or low boiling point liquid inside, for four different blocked lengths (l_1 = 2.5 mm, l_2 = 7.5 mm, l_3 = 12.5 mm, and l_4 = 17.5 mm). The actuator is similar to the one shown in Figure 1, but it has less segments, therefore, and a shorter length (maximum length is ≈1.8 cm, compared to ≈2.5 cm of the actuator in Figure 1). If it is assumed that the contact surface area is constant for a given length, the force and pressure relationship can be expressed by the linear relationship $F = \Delta P \cdot A$. Here, F is force, ΔP is pressure difference, and A is surface area of the inflatable portions of the approximately cylindrical actuator. The blue, yellow, green, and red circles in Figure 4a show the experimental data and the black solid lines show linear fits to the experimental data. Calculated effective contact areas can be seen in Figure 4b. The effective contact area decreases with increasing length as seen in Figure 4b, as a result of the shape deformation of the surface. The diameter of the effective contact circle is found to be 2.1 cm by the linear model for l_1 = 2.5 mm, which matches reasonably with the measured diameter of 1.9 cm.

To estimate the volume of the space in the actuator, a controllable volume is added by using a syringe and the blocked force

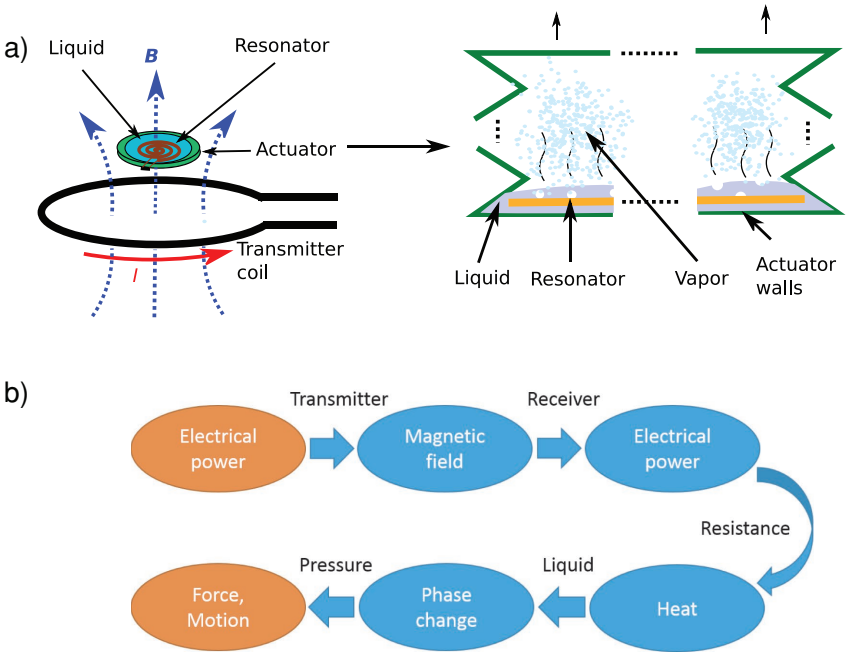

Figure 2. Wireless actuation by phase change. Electrical power is used to produce magnetic field shown by B) for wireless power transmission and the received electrical power is used to heat the liquid for phase change to obtain force and/or motion. a) Illustration of the wireless actuation concept. b) Energy flow during wireless actuation.

F is measured by changing this additional volume, V_{syr} (see Figure 4c). This is done for three different lengths $d_1 \approx 2$ mm, $d_2 \approx 7.5$ mm, and $d_3 \approx 13$ mm. In the calculation of the actuator volume, the first step is to find the effective contact areas corresponding to the given lengths, by the data in Figure 4b. Once the effective areas are found, the force data can be converted to a pressure difference between the inside and outside of the actuator. In the second step, the closed actuator and syringe system is assumed to obey the ideal gas law:$(\Delta P + P_{atm}) \cdot V_{tot} = n_{tot} \cdot R_{gas} \cdot T$, where P_{atm} is atmospheric pressure, (ΔP + P_{atm}) is the inner pressure, V_{tot} is the total volume (actuator and syringe), n_{tot} is the mole number of the gas inside, T is temperature in K, and R_{gas} is a constant. The red dashed curves in Figure 4c show the ideal gas model fits obtained by constant n_{tot} and T assumptions. The calculated inner space volumes of the actuator are 4.85, 6.3, and 6.4 mL for d_1, d_2, and d_3, respectively.

To characterize the wireless version of the actuators, a coil (inductance and resistance measured at 100 kHz are 15.86 µH and 3.31 Ω, respectively) and ≈0.6 mL liquid (3M NOVEC 7000 Engineered Fluid) is placed in the actuator and the coil is connected to a capacitor (measured to be 45.7 nF) to form a resonator (see **Figure 5**a). The actuator is placed on top of a large transmitter coil (see the Experimental Section) at a spacing of ≈2 mm.

Figure 5b shows the instantaneous force and power during and after excitations of ≈15 s for different excitation levels. The voltage in the capacitor is measured by connecting a rectifier circuit (diode and capacitor) with a negligible loading effect to convert the sine wave to a DC voltage. The average power dissipated in the resonator during on time is calculated to be in the range of 0.16–1.33 W. The received power is not constant during actuation and this is potentially due to the fact that the coil is free to move in the actuator and also to the shifts in electronic component values because of heat. It is seen that the actuator responds almost immediately to the electrical excitation. Evaporation and condensation processes are rather complex to fully model and go beyond the focus of this paper, therefore, we only provide some basic energy calculations. The energy required to bring 0.6 mL of the liquid from room temperature (22 °C) to the boiling point (34 °C) is found to be 13.1 J. It would take ≈10 s to obtain this energy with 1.33 W power, therefore, the phase change start occurs faster (due to local heating concentrations) than would be expected simply based on bulk uniform heating of the liquid. The energy needed to heat the coil to the boiling temperature of the liquid when the coil is assumed to be isolated is estimated to be less than 0.5 J.

For a force of 7 N for a negligible expansion (less than 1 mm), the energy necessary to boil the gas is calculated to be ≈1 J. This calculation is done as follows: based on the volume and contact

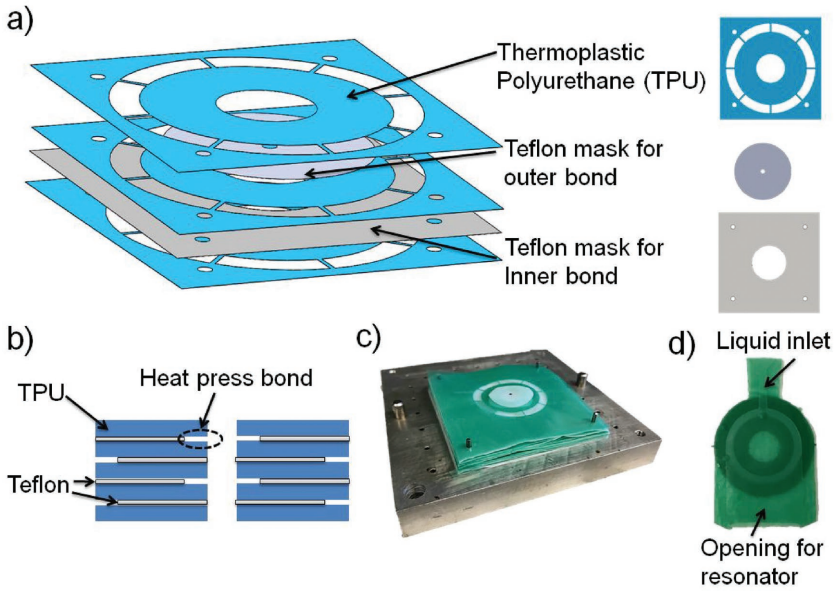

Figure 3. Soft bellow fabrication. a) Stacking up TPU and Teflon layers. b) The bond between the TPU layers occurs where there is no Teflon mask. c) The layers are aligned with dowel pins and precision die plates. d) The bottom layer contains an opening to insert the resonator as well as an inlet for injecting the low evaporation point liquid.

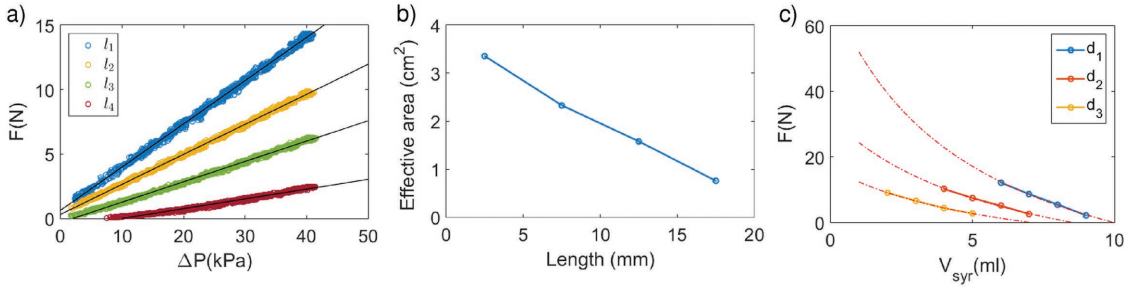

Figure 4. Relationship between force and pressure difference for various lengths, effective contact areas calculated from this data, and effective volume estimation. a) Force versus inner pressure (relative to external pressure) for four different lengths in blocked states (l_1 = 2.5 mm, l_2 = 7.5 mm, l_3 = 12.5 mm, and l_4 = 17.5 mm). It is seen that there is a linear relationship between force and pressure difference, as expected. Black lines show linear fits. b) Effective area versus length, l. Effective contact area decreases with increasing expansion due to the shape deformation in the actuator. The corresponding effective contact diameter for l_1 = 2.5 mm is calculated to be 2.1 cm, whereas the diameter of the inflatable sections of the actuator are measured to be ≈1.9 cm. c) Effective actuator volume estimation. The blocked force (F) is measured for different volumes in a syringe connected to the actuator (V_{syr}) for three different lengths, i.e., $d_1 \approx 2$ mm, $d_2 \approx 7.5$ mm, and $d_3 \approx 13$ mm.

area information (see Figure 4), the necessary pressure difference to produce the desired force for a given length is found and this pressure difference is used to calculate the amount of the gas required by the ideal gas law. After finding the mass of the required gas, the energy to boil the liquid is calculated.

It is seen that the force increase follows a linear trend for actuation conditions (actuation duration, power level, etc.) as shown in Figure 5b. This shows that it can be assumed that the power transferred to the liquid produces an approximately constant amount of gas per unit time. In Figure 5c, we see a periodic actuation with durations of ≈15 s and relaxation durations of ≈30 s. Since subsequent actuation cycles occur before complete relaxation, there is a tendency of the force to increase over several cycles. However, this may be minimized by optimization of actuation-relaxation durations and upper–lower limits for the forces, if the application permits. To see the trend of the force on the input power clearly, the maximum forces in Figure 5b are plotted against the average power in the actuation

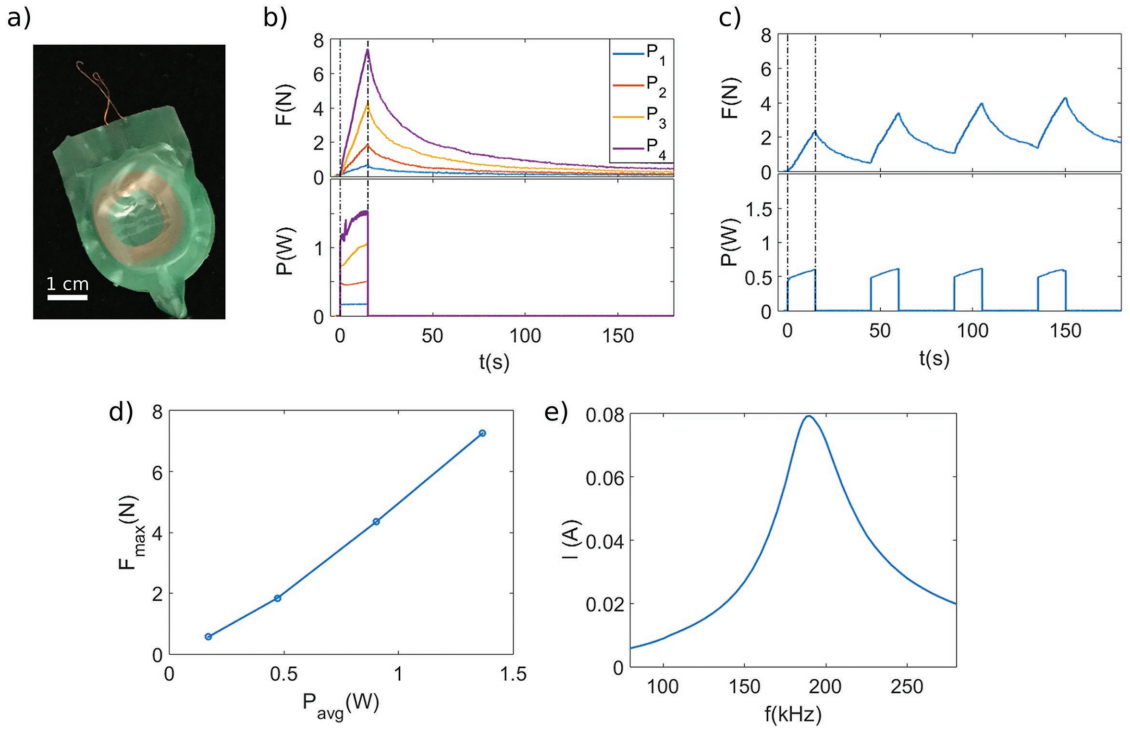

Figure 5. Characterization of the wireless actuator. a) Bellows-style actuator with an embedded coil. A capacitor is connected to the coil externally to complete the resonator. b) Blocked force and power versus time for different excitation levels. The transmitter currents corresponding to the levels P_1, P_2, P_3, and P_4 are I_1 = 0.81, I_2 = 1.47, I_3 = 1.97, and I_4 = 2.5 A root mean square (RMS), respectively. c) Blocked force and power versus time in a periodic actuation. The on time is 15 s and the off time 30 s. A slight force increase is seen after each cycle as a result of incomplete relaxation. d) Maximum forces in Figure 5b versus average power during the actuation phases. e) The current in the resonator versus excitation frequency at a relatively low power level (less than 50 mW dissipated in the resonator).

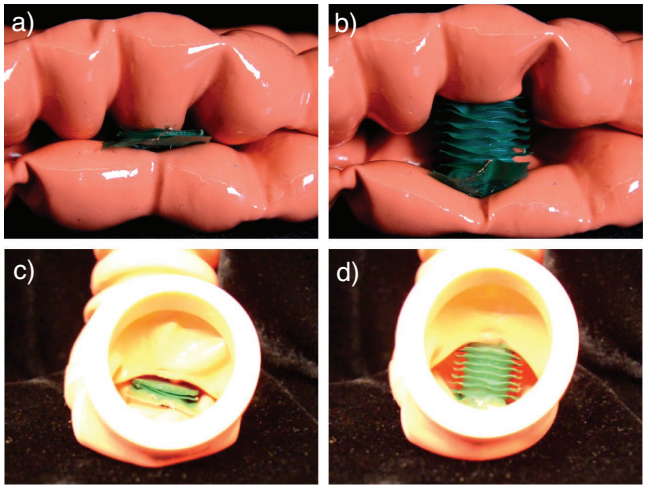

Figure 6. Wireless ultrastrong and soft actuators have the potential to be used in different tasks including wireless organ manipulation (e.g., separation) and to open blocked channels. a) Before actuation. b) During actuation. c) Before actuation. d) During actuation.

duration (Figure 5d). It is seen that there is an approximately linear dependence between these two quantities as expected. From the data shown in Figure 5b, if we assume that 7.5 N of blocked force is obtained in 15 s and given that the maximum displacement is ≈1.8 cm, we can estimate the mechanical power output by $0.5 \times 7.5\ \text{N} \times 1.8\ \text{cm}/15\ \text{s}$, which gives several mW. This means that the electrical to mechanical power conversion efficiency is less than 1% - low, as expected due to the thermal nature of the actuation process. The volume change when the actuator is free to move can be understood by the ideal gas law, $(\Delta P + P_{\text{atm}}) \cdot V_{\text{act}} = n_{\text{gas}} \cdot R_{\text{gas}} \cdot T$. As seen in this expression, the volume will increase linearly with increasing mole number of the internal gas. Therefore, a similar behavior to blocked forces can be expected, assuming a constant boiling point. Figure S1 in the Supporting Information shows an example of an expansion which has a linear relation to the energy input, similar to the force. We can see the induced current in the resonator in the actuator versus frequency of the applied field in Figure 5e. This is the complete response of the system, which means that the excitation variation is also included in the induced current.

3. Discussion

In this work, we present a concept for wireless soft actuators. The presented actuators use liquid–gas phase change triggered by wireless resonant power transmission and can exhibit ultrahigh forces and large expansions in an extremely light and thin form factor. Despite their relatively low speed, they can find applications in various areas such as biomedical devices, by exploiting the large design space in terms of materials and forms that are compatible with this concept.

An exciting development at the intersection of medicine and robotics is robotic surgery, which tries to minimize the damage to the body by minimizing the size and number of incisions. To achieve this, the number of wires/tubes going into the human body is tried to be minimized. From the perspective of surgeon, this could enable more dexterous and capable surgical operations, and from the patient side, less invasive procedures could decrease complications, pain, and recovery time. The wireless actuation concept introduced here has the potential to close the gap of wireless actuators which can offer assistance to surgeons, for example to manipulate tissue and organs with strong forces and soft interactions with minimal damage. In an intestine model (**Figure 6** and Movies S2 and S3, Supporting Information) we demonstrated two potential examples, where the wireless bellows actuator manipulates phantom organs in various scenarios, such as to open space for surgical tools, or to enlarge channels for reasons such as recovery of flow or to obtain better views. It is notable that the boiling point (at 1 atm) of the liquid used here is less than the internal temperature of the human body, precluding applications for internal medicine. For biomedical applications, further study is needed to develop a biocompatible liquid with a slightly higher boiling point.

4. Experimental Section

Actuator: The thickness of TPU sheets used is 38.1 µm and the thickness of the masks, made of PTFE/Teflon, is 50.8 µm. The CO_2 laser used is made by Universal Laser Systems, Inc., Scottsdale, Arizona, USA and the impulse heat sealer is AIE-410FL by American International Electric Inc., City of Industry, California, USA.

External Field: The external magnetic field is produced by a coil connected to a power amplifier, of which the input is provided by an arbitrary waveform generator which can be controlled by a computer. The source coil used in the characterization is a planar spiral coil with approximately nine turns, inner radius of 0.94 cm, and outer radius of 3.3 cm. The source coil used in the demonstrations shown in Figure 6 is a circular coil with ≈25–30 turns and a radius of ≈6 cm. It is connected to the power amplifier through matching capacitors. Using a larger coil with more turns increases the spatial range of the system whereas using a passive static capacitive matching circuit decreases the bandwidth. The power dissipated by the transmitter coil in characterization is estimated to be less than 50 mW. When larger coils with higher number of turns are used as the source coil, this value increases. In our demonstration experiments, the power dissipated by the transmitter coil with a radius of ≈6 cm is estimated to be several watts.

The strength of the external magnetic field applied to the actuator in the experiments is estimated to be on the order of several hundred µT and the actuator could be actuated at a distance of ≈4 cm from the larger transmitter coil in the setup. The experimental characterizations were performed at very small distances, on the order of several millimeters. More details about the magnetic field profile of the source coil used in the characterization can be seen in an earlier study.[23] The final configuration and design (e.g., geometry and placement of coils in and around the body, resonant frequency, duration of excitation, etc.) would depend on the application, exposure limitations, and electromagnetic interference with other devices around.

Supporting Information

Supporting Information is available from the Wiley Online Library or from the author.

Acknowledgements

The authors acknowledge the support from the Wyss Institute for Biologically Inspired Engineering. Furthermore, M.B. acknowledges the support by Swiss National Science Foundation through the Early Postdoc

Mobility Fellowship. The authors thank Joshua Gafford, Enes Taylan, Tomasso Ranzani, Sheila Russo, and Asli Atalay for useful discussions.

Conflict of Interest

The authors declare no conflict of interest.

Keywords

phase change, pneumatic, wireless soft actuators

Received: August 23, 2018
Published online: October 22, 2018

[1] K. Suzumori, S. Iikura, H. Tanaka, *Proc. IEEE Int. Conf. Robot. Autom.*, Vol. *2*, IEEE, Sacramento, CA, USA **1991**, pp. 1622–1627.
[2] S. Wakimoto, K. Ogura, K. Suzumori, Y. Nishioka, *IEEE Int. Conf. Robot. Autom.*, IEEE, Kobe, Japan **2009**, pp. 556–561.
[3] R. F. Shepherd, F. Ilievski, W. Choi, S. A. Morin, A. A. Stokes, A. D. Mazzeo, X. Chen, M. Wang, G. M. Whitesides, *Proc. Natl. Acad. Sci. USA* **2011**, *108*, 20400.
[4] F. Ilievski, A. D. Mazzeo, R. F. Shepherd, X. Chen, G. M. Whitesides, *Angew. Chem., Int. Ed.* **2011**, *50*, 1890.
[5] M. T. Tolley, R. F. Shepherd, B. Mosadegh, K. C. Galloway, M. Wehner, M. Karpelson, R. J. Wood, G. M. Whitesides, *Soft Rob.* **2014**, *1*, 213.
[6] D. Rus, M. T. Tolley, *Nature* **2015**, *521*, 467.
[7] L. Hines, K. Petersen, G. Z. Lum, M. Sitti, *Adv. Mater.* **2017**, *29*, 1603483.
[8] S. Li, D. M. Vogt, D. Rus, R. J. Wood, *Proc. Natl. Acad. Sci. USA* **2017**, *114*, 201713450.
[9] K. Suzumori, A. Wada, S. Wakimoto, *Sens. Actuators, A* **2013**, *201*, 148.
[10] T. Akagi, S. Dohta, S. Fujimoto, Y. Tsuji, Y. Fujiwara, *Int. J. Mater. Sci. Eng.* **2015**, *3*, 55.
[11] H. Matsuoka, K. Suzumori, T. Kanda, *ROBOMECH J.* **2016**, *3*, 1.
[12] H. Matsuoka, T. Kanda, S. Wakimoto, K. Suzumori, P. Lambert, *Int. J. Autom. Technol.* **2016**, *10*, 517.
[13] A. Wada, H. Nabae, T. Kitamori, K. Suzumori, *Sens. Actuators, A* **2016**, *249*, 1.
[14] T. Hiramitsu, A. Wada, K. Suzumori, H. Nabae, G. Endo, *IEEE/SICE Int. Symp. Syst. Integr.*, IEEE, Sapporo, Japan **2016**, pp. 616–621.
[15] T. Kitamori, A. Wada, H. Nabae, K. Suzumori, *IEEE Int. Conf. Intell. Robots Syst.*, **2016**, *2016-Novem*, 543.
[16] K. Nakahara, K. Narumi, R. Niiyama, Y. Kawahara, *IEEE Int. Conf. Rob. Autom.*, IEEE, Singapore **2017**, pp. 1856–1863.
[17] M. Wehner, R. L. Truby, D. J. Fitzgerald, B. Mosadegh, G. M. Whitesides, J. A. Lewis, R. J. Wood, *Nature* **2016**, *536*, 451.
[18] N. W. Bartlett, M. T. Tolley, J. T. B. Overvelde, J. C. Weaver, B. Mosadegh, K. Bertoldi, G. M. Whitesides, R. J. Wood, *Science* **2015**, *349*, 161.
[19] A. Miriyev, K. Stack, H. Lipson, *Nat. Commun.* **2017**, *8*, 596.
[20] J. J. Abbott, K. E. Peyer, M. C. Lagomarsino, L. Zhang, L. Dong, I. K. Kaliakatsos, B. J. Nelson, *Int. J. Rob. Res.* **2009**, *28*, 1434.
[21] M. Sitti, *Nature* **2009**, *458*, 1121.
[22] M. Boyvat, C. Hafner, J. Leuthold, *Sci. Rep.* **2014**, *4*, 5681.
[23] M. Boyvat, J.-S. Koh, R. J. Wood, *Sci. Rob.* **2017**, *2*, eaan1544.
[24] T. Ranzani, S. Russo, F. Schwab, C. J. Walsh, R. J. Wood, *IEEE Int. Conf. Robot. Autom.*, IEEE, Singapore **2017**, pp. 1125–1131.

